Chapter 3

Form Factors

3.1 Models and fits

While the theory for strong interactions, QCD, is well known, because of confinement it is impossible to use perturbative techniques to do calculations at low Q^2. Since it is low Q^2 that is pertinent to the structure of hadrons, approximate models must be used to understand this physics. Understanding the form factors, especially G_E^n since it is relatively unknown, provides assistance in understanding nuclear structure. Models have been developed to describe the structure of hadrons, and data is needed to determine which models provide a better description.

There are a large number of models of nuclear form factors, a few classes of which will be discussed here. Although lattice QCD has the most long term promise for understanding the physics of strong interactions, since the comparison of the results with data will show the current limitation in computing power, they will not be included.

3.1.1 Fits

In the early studies of nucleon form factors, a phenomenological fit was performed to determine the behavior of G_E^n, based upon unpolarized data and the Rosenbluth technique. This fit of the data is known as the Galster parameteriza-

tion, and is

$$G_E^n(Q^2) = -\frac{\mu_n}{1+5.6\tau} G_D(Q^2), \tag{3.1}$$

where G_D is the dipole form factor

$$G_D = \frac{1}{(1+\frac{Q^2}{0.71})^2} \ . \tag{3.2}$$

The other three form factors (G_E^p, $\frac{G_M^p}{\mu_p}$, $\frac{G_M^n}{\mu_p}$) all show good agreement G_D using data acquired from the Rosenbluth method. As new data have become available, this simple fit has been updated. See for example the fit by Kelly [**?**].

3.1.2 Vector meson dominance model

A representative vector dominance model which is in reasonable agreement with the low Q^2 data is one by Bijker *et al.*[10] This model has pQCD scaling relations built into the fit, and a phenomenological contribution attributed to the nucleon's qqq structure. The added term for F_2^V is $\frac{g(Q^2)}{1+\gamma Q^2}$ introduced to reflect pQCD. The intrinsic form factor used was $g(Q^2) = (1+\gamma Q^2)^{-2}$.

Another representative model, by Lomon *et al.*, also included meson pole terms and a term with pQCD behavior. This model also includes the additional vector mesons of ρ' and ω' compared to the previously described one, requiring a total of 14 free parameters [42].

3.1.3 Pion cloud and CQM

Miller, *et al.*, expanded the constituent quark model into the light-front cloudy bag model [45]. Here the three relativistic constituent quarks are surrounded by a

nonrelativistic cloud of pions. Poincaré invariance provides an additional constraint needed to fit the G_E^n data. This model has recently been expanded into the light front cloudy bag model, with the pion cloud contributing through a relativistic π-nucleon form factor. The corrected form factors are in terms of the form factors without relativistic effects, and the virtual pion four momentum. An additional parameter is introduced in the π-nucleon form factor, for the relativitistic correction[45].

3.1.4 Model of Generalized Parton Distributions

The interest in GPDs recently have led to several models being developed. Among these are models by Guidal *et al.*[28][50] and Diehl *et al.* [20]. In these models, the GPD framework is used to describe observables which are independent of skewness ξ (see Figure 1.1). Guidal *et al.* parameterize the GPDs in the following way

$$H^q_{R2}(x,0,Q^2) = q_v(x)x^{\alpha'(1-x)Q^2} \ , \tag{3.3}$$

$$E^q_{R2}(x,0,Q^2) = \frac{\kappa^q}{N^q}(1-x)^{\eta^q} q_\nu(x)x^{\alpha'(1-x)Q^2} \ . \tag{3.4}$$

Here the α' is the universal Regge slope, while the η^q govern the behavior for the helicity-flip GPDs as x approaches 1. This was added to produce a faster falloff at large Q^2 in the $x \to 1$ limit. The model by Diehl *et al.* is described in Section 6.4.2.

3.1.5 pQCD predictions

As stated in section 1.2.1, perturbative QCD gives the prediction that [7]

$$F_1 \propto \frac{1}{Q^4} \ . \tag{3.5}$$

This relationship is also expected to be relevant at moderate Q^2 when higher order QCD terms are included, which treat small-x partons better. The small quark masses mean that the dominant mechanism for helicity flip in QCD comes from the quark orbital angular momentum. Generalized power counting including this orbital angular momentum gives a scaling of

$$F_2 \propto \frac{1}{Q^6} \ . \tag{3.6}$$

This behavior depends on the leading order and next to leading order light-cone wave functions, the latter dominated by the probability amplitude for one quark to carry one unit of orbital angular momentum. It is suggested that the higher order resummation suppresses the low x contribution, providing an effective cut off for the integrals is at $x \approx \ln^2(\Lambda^2/Q^2)$ [7].

$$\frac{F_2}{F_1} \propto \frac{\ln^2 \frac{Q^2}{\Lambda^2}}{Q^2} \ . \tag{3.7}$$

Here Λ is the QCD renormalization scale. While this scaling relation is accurate for the proton, a rough calculation of $Q^6 F_2(Q^2)$ gives about $\frac{1}{3}$ the value of experimental data for $Q^2 < 5$ GeV^2 [7].

3.2 Measuring GEn via the Rosenbluth technique

As mentioned earlier, equation 2.35 suggests one technique to determine the electric and magnetic form factors. By carrying out multiple measurements at different angles for a given Q^2 the two components of the cross section may be independently determined, allowing a separation of the electric and magnetic form

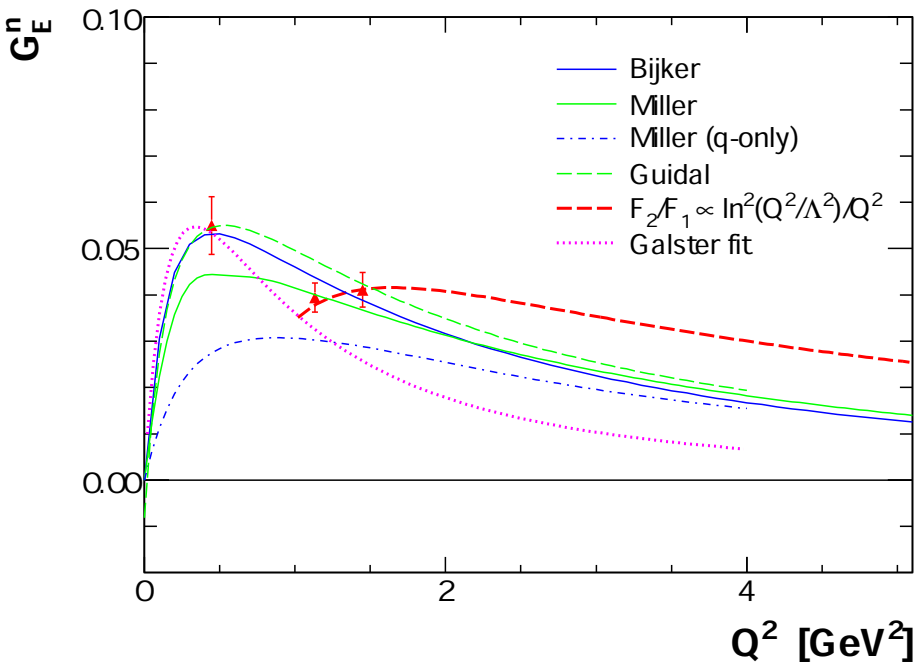

Figure 3.1: Various fits discussed in the text. The points plotted are from [43], which was used to fit the pQCD curve. These data are only representative, see figure 3.2 for the full set. The Bijker curve is a representative Vector Meson Dominance model, the Guidal curve is a representative GPD based model, the Miller curves are from a CQM.

factors. This technique is known as Rosenbluth separation. Experiments to measure the electric form factor of the neutron that use this Rosenbluth method fall into two categories: those in which the impulse approximation for quasi-elastic electron deuteron scattering with the Rosenbluth method is applied directly to the neutron component, and those where the Rosenbluth method is applied to the deuteron through elastic scattering, and an NN model is use to extract a value for G_E^n[37]. The latter is described first.

3.2.1 Elastic e-D scattering

The deuteron, containing two nucleons, is spin-1. Because of this, the equation for the elastic cross section has three form factors, the magnetic G_M, the charged G_C, and the quadrupole term G_Q [51]:

$$\frac{d\sigma}{d\Omega} = \frac{d\sigma_{Mott}}{d\Omega}[G_C^2 + \frac{8}{9}\tau^2 G_Q^2 + \frac{2}{3}\tau(1+\tau)G_M^2 + \frac{4}{3}\tau(1+\tau)^2 G_M^2 \tan^2\frac{\theta_e}{2}] \ . \qquad (3.8)$$

While the θ_e dependence allows G_M to be separated out, the charged and quadrupole terms cannot be separated using the Rosenbluth technique. In addition, it is the coherent sum of proton and neutron electric form factors which is extracted ($G_E^p + G_E^n$). Both of these complications add to the uncertainty in the determination of G_E^n. The electric form factors must be "unfolded" from G_C and G_Q using a model, which makes the results of this technique dependent on the model of the deuteron's wave function [50] [58]. The most recent extraction uses high precision data for G_C, and the Arenhovel model of the deuteron [**?**] [**?**].

3.2.2 Quasi-elastic scattering and the Rosenbluth Technique

Recalling equation 2.16, a technique using quasi-elastic scattering off a nucelon rather than elastic scattering off a deuteron and the Rosenbluth formula (equation 2.35) directly presents itself. By subtracting the cross section of the proton from that of the deuteron, or by measuring the neutron in coincidence with the electron, at the quasi-elastic peak, the cross section of the neutron remains. Then the Rosenbluth formula can be used to arrive at a value for G_E^n.

Most commonly the neutron is detected in coincidence with the scattered electron, to identify that the interaction was with the neutron. However, this technique has also been performed with anti-coincidence measurements, where "no proton" is required in coincidence with the electron [51]. An additional technique used is to measure the ratio of the neutron to proton production cross sections in the electrodisintegration the deuteron. This method has worked very well for the neutron magnetic form factor.

There have been some serious difficulties with these types of experiments. Among these are a heavy dependence on the proton form factors and the aforementioned problems with the Impulse Approximation (section 2.4.1). Additionally, coincidence and anti-coincidence experiments depend on the absolute detection efficiency, which is difficult to determine for neutrons [51].

3.2.3 Difficulties with Rosenbluth method

The uncertainties for these measurements based upon unpolarized quasi-elastic scattering from deuterium are too large to give a definitive nonzero measurement of G_E^n. The dependence on the proton form factors and the uncertainty directly from IA dominate the measurement.

The Rosenbluth technique has another inherent problem: the magnetic form factor is much larger than the electric form factor for the neutron, and the ratio $(\frac{G_E}{\tau G_M})^2$ becomes smaller as the transferred momentum increases. This means that the electric form factor is difficult to decouple from the magnetic form factor, since both the tangential and constant (relative to angle) portions of the cross section are proportional to G_M^2 [62].

3.3 Double polarization techniques

With the difficulties in measuring the electric form factor of the neutron using the Rosenbluth method, new techniques have been sought. Following the suggestion of Arnold, Carlson, and Gross [5] a technique using a longitudinally polarized beam and a recoil polarized neutron has been investigated. The most obvious reaction for such an experiment would be ${}^2H(\overrightarrow{e}, e'\overrightarrow{n})p$.

The most important advantage is that the measured term is proportional to $G_E^n G_M^n$ instead of $(G_E^n)^2$. Additionally, only one measurement is needed for a given Q^2 if all interesting components can be measured.

As mentioned earlier, polarized targets can allow the same physics to be ac-

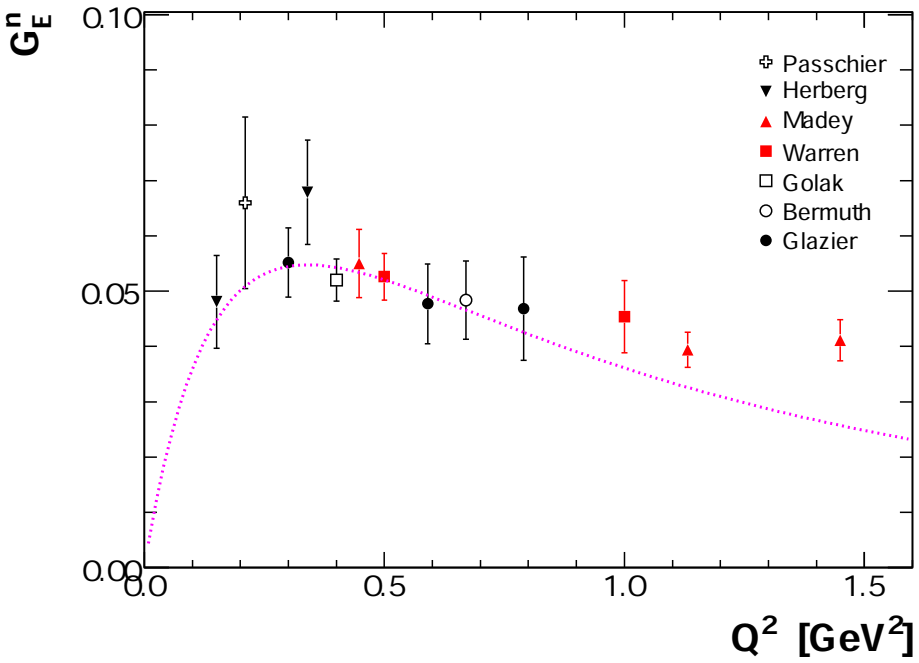

Figure 3.2: Previous G_E^n data from experiments involving polarization techniques. The curve is the Galster parametrization [**?**]. Herberg provided new calculations of the Ostrick data, while Golak provided a FSI corrected analysis of the Becker data. For references see Table 3.3.

cessed as detecting a polarized recoil neutron. Experiments have been carried out with either recoil polarization, where the polarized neutron is detected in a polarimeter, or with a polarized target, either polarized deuterium or polarized ^{3}He, with a detected unpolarized neutron[43]. Table 3.3 contains a summary of recent experiments all of these techniques.

All experiments using the double polarization technique are dependent on a helicity dependent experimental asymmetry,

$$A_{exp} = \frac{N_+ - N_-}{N_+ + N_-} \ , \tag{3.9}$$

which can then be related to G_E^n. Here N_+ gives the number of events with helicity aligned with the nucleon polarization or with the beam direction and N_- gives the number of events with helicity with the opposite sign compared to nucleon polarization or against the beam direction.

3.3.1 Quasi-elastic scattering and (e,e'n)

For PWIA to be applicable, quasi-elastic events must be selected. Even though the cross section is not being measured, the process of selection of these events is important, as double polarization techniques depend on asymmetries, which are diluted by events which are not part of the desired asymmetry. Two useful quantities for selecting quasi-elastic events in coincidence experiments are the missing energy (defined by $E_m = m_f + m_B - m_{A+i}$ with A, B, i, and f as shown in figure 2.2) and the missing momentum (defined by $\mathbf{p}_m = \mathbf{p}_i - \mathbf{q}$).

In the experiments that have been carried out to date, the experimental trig-

Q^2	$Date$	$Reference$	$target$
0.16	1991	Jones-Woodward[34]	$^3\overrightarrow{\mathrm{He}}$
0.2	1992	Thompson[65]	$^3\mathrm{He}$
0.31	1994	Meyerhoff[44]	$^3\overrightarrow{\mathrm{He}}$
0.255	1994	Eden[23]	$^2\mathrm{H}$
0.15, .34	1999	Ostrick[48]	$^2\mathrm{H}$
0.4	1999	Becker[6]	$^3\overrightarrow{\mathrm{He}}$
0.21	1999	Passchier[49]	$^2\overrightarrow{\mathrm{H}}$
0.67	1999	Rohe[58]	$^3\overrightarrow{\mathrm{He}}$
0.45, 1.13, 1.45	2003	Madey[43]	$^2\mathrm{H}$
0.5, 1	2003	Warren[66]	$^2\overrightarrow{\mathrm{H}}$
0.3,0.6,0.8	2003	Glazier[26]	$^2\mathrm{H}$
0.67	2003	Bermuth [8]	$^3\overrightarrow{\mathrm{He}}$

Table 3.1: Double polarization experiments to measure the electric form factor of the neutron that have been carried out to date[51].

ger was typically formed by coincidence between the scattered electron and recoiling neutron. The electrons were detected in a spectrometer or granulated calorimeter. The measured electron kinematics, in concert with large solid angle neutron detectors, allow for event-by-event reconstruction of the particle tracks. For the neutron detector, in higher Q^2 experiments a multi-plane neutron detector was used, with a layer or two of veto detectors in front. In other experiments, two separated layers of scintillator were used, with each layer having veto detectors in front. Veto detectors and time of flight provided neutron identification.

Recoil polarimetry experiments required a different detection scheme in order to detect the polarization of the neutron, as it leaves the target. Polarimeters were set up to measure the "up-down" scattering asymmetry due to the transverse component of the recoil polarization. The polarimeters included a plastic or mineral oil scintillator which determined the neutron time of flight (TOF), and also served as a scatterer, with the polarized scattering exhibiting an asymmetry that was measured in a second set of scintillators. Since the spin vector of the neutron could have any combination of longitudinal and transverse polarizations, a dipole magnet was sometimes used to precess the neutron's spin vector.

These detectors provided scattering angles for both neutrons and electrons. The momentum of the particle(s) provides the needed fifth quantity to select quasi-free (e, n) scattering, and is determined by considering the time of flight (TOF) for the particle(s). A missing signal in the veto detectors along with the determination of the flight time of the particle from the target to the detector provided neutron detection. Additionally, pulse heights in the neutron detector scintillators can be

used to filter out accidental and inelastic events. Quasi-elastic events can also be selected by comparing the expected time of flight (from the electron energy and the angles) to the measured time of flight.

Other events, which dilute the quasi-elastic neutron events, were one of the main sources of uncertainty in these measurements. A major source of background is proton to neutron conversion in the shielding in front of the neutron detectors. This can be minimized with a tight time of flight cut at low hadron momentum. Good time resolution also allows removal of pion events, another source of dilution. Monte Carlo simulations have been used to determine the proper dilution factor from the uncertainties and to average out the theoretical asymmetries and the effects of finite acceptance.

3.3.2 Recoil polarimetry

Four experiments used recoil polarization techniques to measure G_E^n. These experiments were Madey *et al.*[43] in Hall C at Jefferson Lab, Glazier *et al.*[26] at the Mainz Micotron, Ostrick *et al.*[48] at the Mainz Microtron, and Eden *et al.*[23] at the MIT-Bates laboratory. The first three named experiments (Eden *et al.* was a proof of concept experiment) produced published data.

In these experiments, neutrons were produced through electrodisintegration of deuterons in an unpolarized liquit deuterium target using longitudinally polarized electrons. Contamination from hydrogen within such targets was found to be small[23] [43].

From equations 2.26 and 2.28 we can develop a relationship between the ratio of the components of polarization, and the ratio of the form factors

$$\frac{G_E}{G_M} = -\frac{P_x}{P_z}\frac{E_i + E_f}{2M}\tan\frac{\theta_e}{2} \ . \tag{3.10}$$

Here P_x and P_z are the x and z components of polarization. In order to determine the up-down asymmetry A_{meas} must be observed. It follows a sinusoidal dependence

$$A_{meas} = A_y|\overrightarrow{P}|\sin(\chi + \chi_0) \ . \tag{3.11}$$

Here A_y is the beam analyzing power, and χ is the spin precision angle, of the detected particle as it travels through a magnetic field.

$$\tan\chi_0 = \frac{P_x}{P_z} = -\frac{G_E}{G_M}\frac{\cos\frac{\theta_e}{2}}{\sqrt{\tau + \tau^2\sin^2\frac{\theta_e}{2}}} \ . \tag{3.12}$$

Using this spin precision technique removes the need for absolute calibration of the electron beam polarization and effective analyzing power [52].

Arenhovel[4][3] showed that for a deuteron target, corrections due to meson exchange currents and isobar configurations are small, and these have little dependence on Q^2. It was found, however, that especially at lower values of Q^2, effects from final state interactions (FSI) can play a large role [48].

Ostrick *et al.* found at $Q^2 = 0.35$ GeV^2 that the neutron polarization was reduced by less than 4% due to FSI effects, but at $Q^2 = 0.12$ GeV^2 the transverse polarization is reduced by 50%. These final state interactions were calculated to mostly arise from $p - n$ charge exchange via pion exchange. A model was used to calculate the change to the polarization by FSI, and a correction was applied [48].

Glazier *et al.* found that at neutron energies of a few hundred MeV the scattering in the polarimeter was dominated by quasi-elastic scattering, which added to the effective analyzing power of the polarimeter. This means that A_{meas}, the effective asymmetry, could not be computed accurately, and the statistical precision was not exactly known[26].

Madey *et al.* also used a cross ratio technique, which makes the neutron polarimeter results independent of any luminosity change based on beam helicity, as well as of the efficiencies and acceptances of the two halves of the polarimeter. This experiment used a different technique to account for FSI effects. By using possible G_E^n values in a simulation, the neutron polarization was calculated which was then compared to experiment[43].

3.3.3 Polarized target measurement

To measure G_E^n using a polarized target, we measure the asymmetry A

$$A = \frac{\sigma_+ - \sigma_-}{\sigma_+ + \sigma_-} = \frac{\Delta}{\Sigma} \ , \tag{3.13}$$

where $\sigma_\pm$ are the cross sections (Equation 2.38) with electron helicity ± 1. If the polarization direction of the target is flipped, this changes the sign of the asymmetry. This asymmetry is not explicitly measured, but rather

$$A_{meas} = P_e P_t A \ , \tag{3.14}$$

where P_e is the polarization of the electron, P_t is the polarization of the target, and

$$A = -\frac{2\sqrt{\tau(1+\tau)}\left[\tan\frac{\theta_e}{2}\sin\theta\cos\phi G_E^n G_M^n + \sqrt{\tau[1+(1+\tau)\tan^2\frac{\theta_e}{2}]}\cos\theta(G_M^n)^2\right]}{(G_E^n)^2 + \tau[1+2(1+\tau)\tan^2\frac{\theta_e}{2}](G_M^n)^2} \ . \tag{3.15}$$

Here θ and ϕ are the angles defined in Figure 2.3. Setting the angles properly ($\theta = 90°$ and $\phi = 0°$) greatly simplifies things, giving the perpendicular asymmetry:

$$A_\perp = \frac{-2\sqrt{\tau(1+\tau)}\tan\frac{\theta_e}{2}\frac{G_E}{G_M}}{(\frac{G_E}{G_M})^2 + \tau[1 + 2(1+\tau)\tan^2\frac{\theta_e}{2}]}. \tag{3.16}$$

Since the ratio of $\frac{G_E}{G_M}$ is small, the perpendicular asymmetry is roughly proportional to the ratio $\frac{G_E}{G_M}$. The parallel asymmetry can be used to normalize the value, so that:

$$G_E^n = \frac{a}{b} G_M^n \frac{(P_e P_t V)_\parallel A_\perp}{(P_e P_t V)_\perp A_\parallel}, \tag{3.17}$$

where $a = 2\sqrt{\tau(1+\tau)}\sqrt{\tau[1 + (1+\tau)\tan^2\frac{\theta_e}{2}]}$ and $b = 2\sqrt{\tau(1-\tau)}\tan\frac{\theta_e}{2}$.

3.3.4 Experiments with polarized deuterium

Two experiments used polarized deuterium targets to measure the value of G_E^n, one in Hall C at Jefferson Lab (Warren *et al.*[66]) and the other at NIKHEF in Amsterdam, the Netherlands (Passchier *et al.* [49]).

Under PWIA, for deuteron targets with polarization in the scattering plane and after proper averaging of the asymmetry(symmetrically around $\mathbf{q}$), the measured asymmetry is

$$A_{meas} = V \frac{P_e P_1^d A_{ed}^V}{1 + P_2^d A_d^T}\ , \tag{3.18}$$

where V is the dilution factor, P_1^d is the vector polarization, P_2^d is the tensor polarization, A_{ed}^V is the deuteron tensor beam-target asymmetry, and A_d^T is the vector deuteron target asymmetry. For most targets the tensor polarization is small, and that term can be ignored.

In these experiments data were compared to predictions by Arenhovel

In the experiment performed by Warren *et al.*, polarized deuterated ammonia was used as the target. The ammonia granules were submerged in liquid helium and aligned with 5 T magnetic field resulting in a typical polarization of 24%. Good agreement with MC predictions showed that quasi-elastic scattering dominated the scattering reaction. This experiment had a narrow range of acceptance, so it was fairly insensitive to Q^2 dependence [66].

In the experiment performed by Passchier *et al.*, polarized electrons were injected into a recirculating storage ring, allowing for large beam currents. An atomic beam source injected a flux of polarized deuterium atoms into a cell in the storage ring with an electromagnet used to orient the polarization axis. This was created by deuteron atoms in two hyperfine states, with an electromagnet to orient the polarization axis [49].

3.3.5 Experiments with polarized helium-3

Another class of experiments to measure G_E^n have used $^3\overrightarrow{\text{He}}$ as the target. Various experiments were carried out at the Mainz Microtron (MAMI) [6][58][8][44] and at the MIT-Bates laboratory[34][65]. The results presented in [8] include those from the experiment reported in [58]. Additionally, experiment E02-013 is of this type and in early 2006 ran at Jefferson Lab in Hall A. The analysis of this experiment, with data up to $Q^2 = 3.5$ GeV^2, is being presented in this thesis.

Optical pumping techniques are used to polarize the ^{3}He either through metastability exchange where the ^{3}He is pumped directly, or through spin exchange. In the

latter, the valence electron in rubidium is optically pumped and the polarization is transferred to the ^{3}He nucleus through collisions. The polarization process for ^{3}He generally does not take place in the target chamber, rather a pumping chamber is used and the polarized helium-3 diffuses into the target cell or is forced in with a compressor. The polarization vector inside of the ^{3}He target can then be measured with NMR.

One of the advantages of a polarized ^{3}He target is that in the ground state the spins of the protons are to a large extent aligned antiparallel to each other. This means that most of the spin of the helium nucleus is carried by the neutron; the polarization of the neutron is $\approx 86\%$ of the polarization of the nucleus [11]. Further details about polarized ^{3}He targets will be presented in section 4.4.

At low Q^2, the complications due to the nuclear wave function can be accounted for with calculations. However, at $Q^2 > 0.6$ GeV^2 this proves difficult, and extrapolation was used in these earlier experiments. Data for G_M^n is used, or a parametrization, in order to arrive at a value of G_E^n from the experimental asymmetry (equation 3.16). A Monte Carlo simulation was used to determine radiative loss and neutron energy loss before the detector, as well as other corrections.

It is possible to select the kinematics such that the measured asymmetry is expressed as:

$$A_{exp} = P_{beam} P_{target} D_{neutron} V_{other} A_{\perp}. \tag{3.19}$$

Here D accounts for dilution from sources related to the target (such as it not being a free neutron), and V is the dilution caused from other sources and from reactions

other than quasi-elastic scattering. This formula assumes that the angles in equation 3.15 are exactly such that $A_{\parallel} = 0$; in practice this isn't possible.

The experiment performed by Becker *et al.* used circulated ^{3}He which was compressed into the target cell by a Toepler compressor. An experiment using deuterium provided a parallel measurement, using the same equipment, pointed to a significant role for FSI that decreases as Q^2 increases. The work by Golak *et al.* expanded upon the analysis of Becker *et al.* by summing the cross sections before forming asymmetries using Faddeev calculations. It was discovered that even at the quasi-elastic peak FSI effects played a significant role. Using theoretical ratios determined from models and comparing to experimental values, G_E^n was extracted from the FSI corrected results [6][27].

In the experiments performed by Rohe *et al.* and Bermuth *et al.*, the data were accumulated by rotating the target spin so that both $A_{\perp}$ and $A_{\parallel}$ could be measured. The measurement of both parallel and perpendicular asymmetries allowed the measurement of the target analyzing power (A_y) which provided a check on the understanding of FSI effects. These were compared to the calculation by Golak *et al.* and FSI effects caused a 3.4% decrease in the reported value of G_E^n. These FSI effects are primarily caused by the photon coupling to one of the protons followed by charge exchange [58][8].

3.4 Summary of past measurements

These three different double polarization techniques have a variety of advantages over the Rosenbluth method, as described in this chapter. While models are used to make corrections, and for polarized deuterium for the measurement itself, the general method is model independent. The three different, independent, techniques used in double polarization measurements provides a check on the understanding of the different types of corrections required.

Because $^3\overrightarrow{\text{He}}$ behaves similarly to a polarized neutron, and because of the low detection efficiency neutron polarimeters, polarized $^3\overrightarrow{\text{He}}$ experiments provide the best statistical precision for measuring G_E^n. FSI effects are taken into account by models for polarized deuterium and calculations for $^3\overrightarrow{\text{He}}$. Because of the robustness of the deuterium model, FSI effects have traditionally played less of a role in deuterium experiments compared to those using $^3\overrightarrow{\text{He}}$. For the discussion and calculation fo FSI effects in polarized ^{3}He for this experiment, at intermediate Q^2, please see the section 5.7.1.

The completed experiments provided precise enough data to clearly identify a small enhancement in G_E^n at $Q^2 = 0.4$ GeV^2. This enhancement is larger in value than the measurements from the Rosenbluth data. At the highest measured values of G_E^n a noticeable difference between the Rosenbluth and polarized data is seen. This is speculated to be due to incomplete radiative corrections for the Rosenbluth data.

In the past decade, precise measurements of the neutron electric form factor

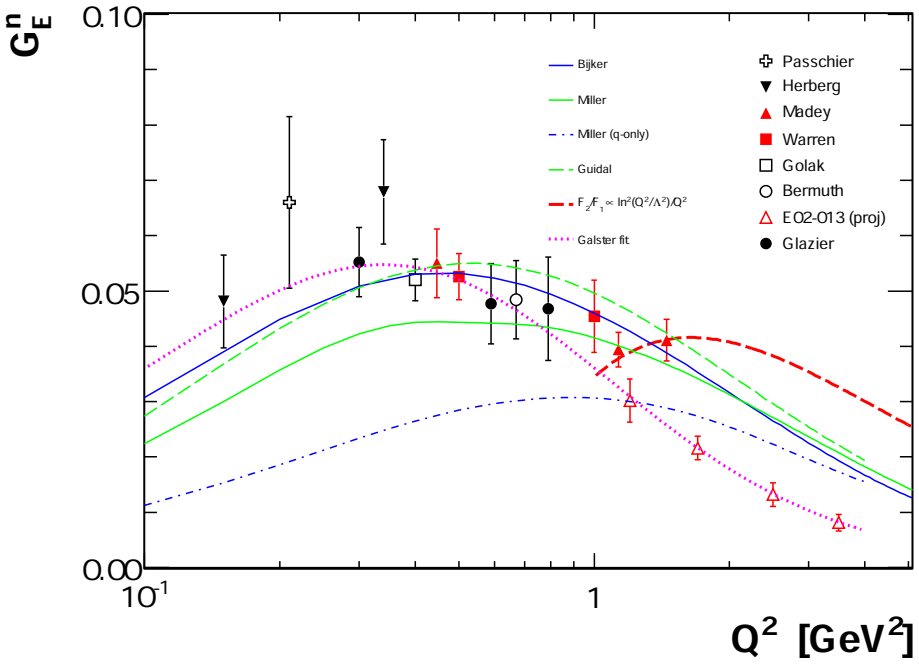

Figure 3.3: Double polarization data and selected models in the region where polarized data is available. Models are described in section 3.1 while data is referenced in Table 3.3.

have become possible and have provided precise knowledge of the structure of nucleons for Q^2 below 1.5 GeV^2. In this region, several models provide a good agreement with the data. The majority of the recent measurements have used the double polarization method, which has the advantage of having greater precision and less model dependence compared to the historic Rosenbluth method.

3.5 E02-013 at Jefferson Lab

As introduced, the physics of nucleons move from the bound behavior described by massive partons, into the behavior described by bare quarks in QCD. There is a complicated transitive region, in the models presented in Section 1.3, that starts at less than 1 GeV and continues to many GeV. The actual point where this behavior changes, and the description of the change, is unknown. In the experiment presented here, the key quantity G_E^n needed to understand nucleon stucture, and behavior such as quark orbital angular momentum, is measured at three separate points in the Q^2 region between 1 and 4 GeV^2.

In this experiment, E02-013, numerous improvements were made to increase the figure of merit (effective statistics) for a measurement in this region. Advances in both instrumentation and in the polarized ^{3}He target technology have been accomplished that enable this measurement. By injecting a small amount of potassium along with the rubidium, the polarization transfer efficiency from the optically pumped rubidium was improved to provide polarizations as high as 50% in the target chamber. The experimental apparatus and target will be explained in detail in

Chapter 4. The value of the asymmetry will be analyzed as a function of $\mathbf{p}_{m,\perp}$, the perpendicular component of the missing momentum, to study FSI effects. A tight cut on $\mathbf{p}_{m,\perp}$ is needed to select low nucleon momenta in the ^{3}He wave function, but also will suppress dilution from proton polarization and FSI interactions. The high Q^2 at which this measurement is undertaken should suppress meson exchange currents. Additionally, meson exchange currents, delta isobar contributions, and finite acceptance effects should be suppressed by a tight cut on $\mathbf{p}_{m,\perp}$[16]. This will be described in detail in Section 5.7.1.